ORIGINAL ARTICLE

# Modulating intracellular acidification by regulating the incubation time of proton caged compounds

**Marilena Carbone**[1,2] · **Gianfranco Sabbatella**[1,3] · **Simonetta Antonaroli**[1] ·
**Viviana Orlando**[4] · **Stefano Biagioni**[4] · **Alessandro Nucara**[5,6]

**Abstract** A proton caged compound, the 1-(2-nitrophenyl)- ethylhexadecyl sulfonate (HDNS), was dosed into HEK-293 at different incubation times. Samples were irradiated with filtered UV light for inducing photolysis of the HDNS and then probed by infrared spectroscopy. The intracellular acidification reaction can be followed by monitoring the consequent $CO_2$ peak intensity variation. The total $CO_2$ produced is similar for all the samples, hence it is only a function of the initial HDNS concentration. The way it is achieved, though, is different for the different incubation times and follows kinetics, which results in a combination of a linear $CO_2$ increase and a steep $CO_2$ increase followed by a decay. This is interpreted in terms of confinement of the HDNS into intracellular vesicles of variable average size and sensitive to UV light when they reach critical dimensions.

## Introduction

Cell life is possible only if intracellular pH ($pH_i$) oscillations are kept within a very narrow range (Lagadic-Gossmann et al. 2004). The intracellular pH is a permissive facilitator of growth and development in normal tissue and in tumors (Pouysségur et al. 1984; Chiche et al. 2010; Boron 2004) and a intracellular $H^+$ load is a indication of high metabolic activity such as respiration.

Manipulating the $pH_i$ in a controlled way implies controlling intracellular processes and activity such as cellular osmotic response (Bourque 2008) and the membrane polarization (Obara et al. 2008) nutrients transport (Thwaites and Anderson 2007).

Cells put in place several mechanisms to regulate pH. High $H^+$ loads are extruded by specialized proteins in the cell membrane and intracellular vesicles through several mechanisms. The $Na^+/H^+$ exchanger (NHE) is an integral plasma membrane protein that mediates the electroneutral exchange of $Na^+$ and $H^+$ in a one-to-one stoichiometry (Orlowski et al. 1992; Harvey and Eherenfeld 1988). Vacuolar-type ATPase is present in the membranes of many organelles, where it exerts a proton or proton-potassium pumping action (Pedersen and Carafoli 1987; Finbow and Harrison 1997). Acid extrusion can also be produced by membrane transporters that load cells with $HCO_3^-$ (or $CO_3^{2-}$) ions (Boron and Boulpaep 1983). These $HCO_3^-$ transport proteins include electroneutral

✉ Marilena Carbone
marilena.carbone@roma2.infn.it

1 Department of Chemical Sciences and Technologies, University of Rome Tor Vergata, Via della Ricerca Scientifica, 1, 00133 Rome, Italy

2 Consorzio Interuniversitario Biostrutture e Biosistemi, Viale Medaglie d'Oro 305, 00136 Rome, Italy

3 Department of Chemistry, University of Rome La Sapienza, P.le A. Moro, 00185 Rome, Italy

4 Department of Biology and Biotechnology "Charles Darwin", University of Rome La Sapienza, P.le A. Moro, 00185 Rome, Italy

5 Department of Physics, University of Rome La Sapienza, P.le A. Moro, 00185 Rome, Italy

6 Center for Life Nano Science, Istituto Italiano di Tecnologia, Viale Regina Elena 291, 00161 Rome, Italy

Na$^+$-HCO$_3^-$ cotransporters (NBC) (Deitmer and Schlue 1989; Choi et al. 2000; Romero et al. 1997) and Na$^+$-dependent and independent Cl$^-$/HCO$_3^-$ exchangers (Wang et al. 2000; Romero et al. 2000; Wong et al. 2002). Extracellular CO$_2$/HCO$_3^-$ buffer facilitates these membrane-transport processes (Hulikova et al. 2011).

The intracellular pH may also be regulated via exogenous compounds, for instance by photoactivated proton caged compounds (PCC), as shown in the recent paper (Carbone et al. 2013). This allowed a high pH jump, which can be easily monitored by infrared spectroscopy. In particular, a long-chained proton caged compound, the 1-(2-nitrophenyl)- ethylhexadecyl sulfonate (HDNS), was purposely synthesized and dosed into 3T3-NIH cells. The dosed cells were then probed by infrared spectroscopy and irradiated by filtered UV light in order to induce intracellular HDNS photolysis. Upon each irradiation, the released protons react with the cytosolic HCO$_3^-$ and release CO$_2$ according to the reactions:

$$H^+ + HCO_3^- \leftrightarrows H_2CO_3 \leftrightarrows H_2O + CO_2 \qquad (1)$$
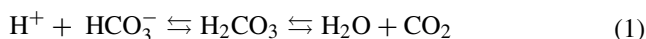
Both HCO$_3^-$ and CO$_2$ peaks may be monitored, however, although the latter appears at 2343 cm$^{-1}$ in a clear region of the cell spectrum and can be clearly singled out, the former is broader and appears around 1360 cm$^{-1}$ in a crowded region of the cell spectrum. Therefore, the detection of the intracellular pH can be achieved by probing the intensity of the CO$_2$ peak. This implies a sufficiently long-lived intracellular CO$_2$ pressure for detecting purposes. A better insight into the CO$_2$ monitoring as outcome of intracellular acidification would improve the application of PCC as exogenous acidification tools. In general, the intracellular level of CO$_2$ is a balance between CO$_2$ influx/efflux and CO$_2$ internal metabolization. In spite of the long-standing assumption that all cell membranes let gases pass extremely easily (Overton 1895) as effect of the high solubility of lipophilic gases in the membranes lipid phase, the CO$_2$ flux is regulated both at the cholesterol level of the membranes (Itel et al. 2012) and by gas-channel proteins (Itel et al. 2012; Kustu and Inwood 2006; Endeward et al. 2008). As for the intracellular metabolization, carbonic anhydrase (CA) is perhaps alone among enzymes in being able to bind CO$_2$ (Dodgson et al. 1980; Chegwidden et al. 2000).

In the current paper, we evaluate the modulation of intracellular pH as a function of the HDNS incubation time on the HEK-293 cells in order to get better insight into the overall PCC-induced intracellular acidification process. The cells are irradiated with UV light and monitored by infrared spectroscopy. We found out that the CO$_2$ produced is similar for all of the samples. The time course of the CO$_2$ integrated peak, however, depends on the incubation time and displays a combination of linear and steep

increases followed by an exponential decay. This finding is interpreted in terms of HDNS confinement into intracellular vesicles of growing size depending on the incubation time and is sensitive to the UV light when reaching a critical average size. Intracellular vesicle explosion frees protons, which generate CO$_2$ according to the equilibrium (1), which is then metabolized by CA/and or gas-channel proteins.

## Materials and methods

### Synthesis of HDNS

HDNS was prepared following the procedure described by Kabalka et al. (1986), with some variations. The synthetic route of the HDNS is reported in the Supplemental Information along with the spectroscopic characterization.

### Cell culture

Human embryonic kidney 293 (HEK-293) cells were cultured directly on UV and infrared-transparent CaF$_2$ windows, in Dulbecco's modified Eagle's medium (DMEM) supplemented with 2 mM glutamine, 10 % FBS, maintained in a humidified incubator at 10 % CO$_2$, and periodically tested to ensure the absence of mycoplasma contamination. Afterwards, the cells were incubated with 2.2 mM HDNS in DMEM for different times (0.5, 1, 2, and 3 h). The cell-coated windows were then transferred to a custom-built sample holder.

### Infrared spectroscopy

FTIR (Fourier-transform infrared) spectroscopy measurements were performed in transmission mode, with a Bruker IFS66/VS interferometer, under vacuum (~$10^{-3}$ mbar), to avoid interference from atmospheric CO$_2$. The cells were housed in a sandwich holder and a 12-μm Mylar spacer was used to control the sample thickness. The signal-to-noise ratio in the 2300–2400 cm$^{-1}$ was 0.5 ÷ 1 %.

### Photolysis and CO$_2$ monitoring

UV radiation (275–375 nm) was provided by a deuterium discharge lamp (Acton Research Corporation) equipped with a band-pass FGUV11 filter (Thorlabs). The power density delivered to the sample is of the order of 0.1 W/mm$^2$. In the photolysis experiment, an area of ca. 7 mm$^2$ was illuminated by UV light. FTIR spectra have been collected with a spectral resolution of 2 cm$^{-1}$. The photoreactivity of HDNS is reported in Fig. 1S of the Supplemental Information. The cells were monitored for a

few minutes by acquiring sequential FTIR spectra in the dark. After confirming stability of the spectra, measurements were interrupted and the cells were irradiated for 1 min with near-UV light. FTIR measurements were then resumed after the irradiated period and repeated at least 20 times before a subsequent irradiation. The spectra are recorded at room temperature and normalized for the first spectrum after the irradiation. The control irradiation of non-dosed cells is reported in the Supplemental Information Fig. 2S.

## Results and discussion

The incubation time of HEK-293 cells with HDNS has a large effect on the modes of $CO_2$ production upon photolysis. This is shown in Fig. 1, where the integrated peak area of $CO_2$ is reported as a function of 0.5, 1-, 2-, and 3-h incubation time, with arrows indicating the irradiation events [panels (a) through (d)]. The irradiation times were chosen after some preliminary tests, so that different kinetics of $CO_2$ production and metabolization as well as mixed kinetic behaviors can be evidenced, in measurements taken in the shortest possible time span. The response of HDNS in DMEM is reported in Fig. 3S. Unlike the cells, the spectral region of the $CO_2$ band appears to be unaffected by the irradiation.

This is interpreted as due to rapid diffusion of photolysis products through the solution, which leads to a too little change of acidity to be detected.

The general behavior of the $CO_2$ integrated intensity after an irradiation event can be described as the combination of a linear increase ($CO_2$-l) and a steep increase followed by a decay ($CO_2$-d), that in some cases follows an exponential behavior. Linear sections and exponential decays were fitted (where possible) and the parameters used are reported in Table 1 along with the associated errors. Furthermore, in Fig. 1, the vertical dashed-dotted lines indicate the ranges taken for the linear fittings.

The 0.5-h sample reaches the maximum level of $CO_2$ production after a few minutes, followed by an exponential decay nearly at the starting level. The time constant of the exponential decay is $242 \pm 8$ s.

The first irradiation of the cells incubated for 1 h causes a linear increase of the $CO_2$ peak area. A second irradiation after 25 min causes $CO_2$ production to reach its peak level followed by a decay, then by a short linear increase again to a level that remains constant also after the third irradiation event. The decay cannot be immediately singled out as exponential, though it can be fitted (with a large error) by the superposition of an exponential decay and a linear increase with the same slope as the first section.

Cells incubated for 2 h and irradiated at 0, 25, and 50 min display a linear increase after the first irradiation event. The second irradiation causes a small steep increase readily metabolized followed again by a linear increase. The third irradiation causes the $CO_2$ to reach its peak level and is followed by a decay to a level slightly higher than prior to the irradiation. The level remains constant also upon the following irradiation. The decays after the steep increases are too sharp and too small for fitting. Therefore, only a linear fitting has been made up to 2600 s, though excluding the points corresponding to the first steep increase (and decay).

The 3-h incubated sample is characterized by a linear increase after each irradiation event until it reaches the saturation level and then remains constant (check was made for a few minutes).

It is noteworthy that only the fraction of $CO_2$ that was generated by a steep increase is subject to the (exponential) decrease. The part of $CO_2$ that is generated according to a linear increase remains constant. As a consequence, the steady intracellular content of $CO_2$ upon HDNS dosing into 293-HEK cells and subsequent irradiations can be related to the incubation time. The slope of the linear sections is different for the different incubation times. A check was made to show that the $CO_2$ variation is not infrared triggered by interrupting the spectroscopic monitoring and retrieving it after a few minutes (region marked with a circle in Fig. 1d). The spectra recorded afterwards were still on the same curve.

### Estimate of total $CO_2$ production

The estimate of total $CO_2$ produced in each of the measurements is straightforward in the 0.5- and 3-h incubation samples. In the former case, it corresponds to the $CO_2$ peak, and in the latter, to the saturation level. For the 1-h sample, it has been considered that the overall $CO_2$ production comprises the peak level reached after the second flash as well as the $CO_2$ generated by linear increase after the decay. This latter contribution is marked in Fig. 1b between two horizontal lines. Similarly, for the 2-h sample, the peak level reached after the third irradiation had been additioned by the fraction of $CO_2$ produced and metabolized after the second irradiation (marked by two horizontal lined in Fig. 1c).

The errors associated are of the order of 4 %, estimated as an average error of 2 % in the $CO_2$ peak integral and another 2 % error in determining the saturation level. The estimated values of total amounts of $CO_2$ production are reported in Table 2.

The total $CO_2$ production is very similar for all samples and can be related to the amount of PCC absorbed by the cells and sensitive to the irradiation.
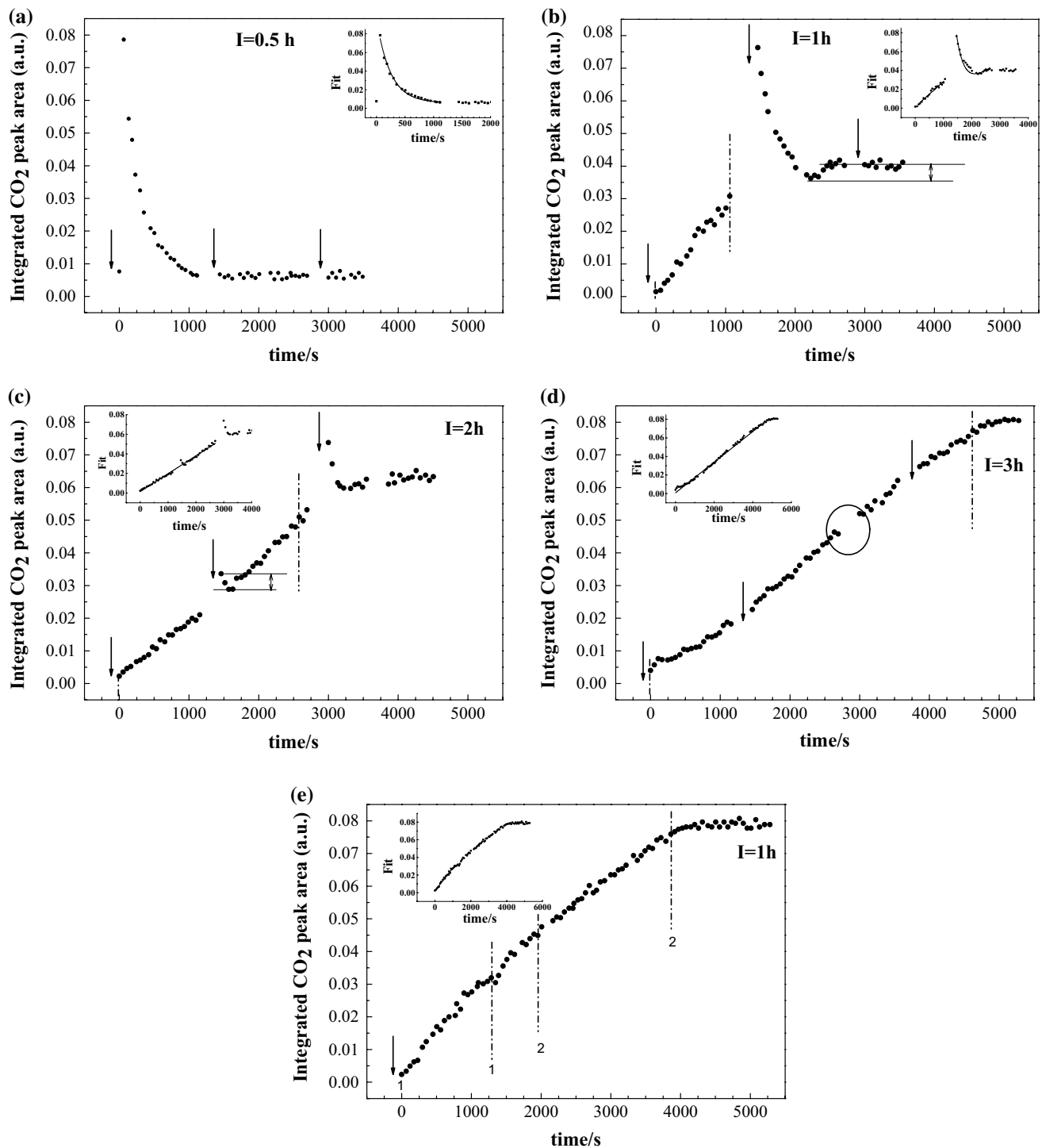
**Fig. 1** Time course of the integrated $CO_2$ peak area after UV-irradiation of the HEK-293 cells dosed with 2.2 mM HDNS at different incubation times: **a** 0.5 h, **b** 1 h, **c** 2 h, and **d** 3 h. The *arrows* indicate the irradiation events. **e** The $CO_2$ integrated peak area of the 1-h incubation samples that underwent a single irradiation event. *I* incubation time. The *vertical dotted-dashed lines* indicate the limits of linear fitting. For the 1-h-1 irradiation, the sample has been fitted with the *lines* in the two intervals marked with 1 and 2 in **e**. The *inset* in each *panel* reports the curves of $CO_2$ with the associated fits. The *horizontal lines* in **b** and **c** correspond to the $CO_2$ to be added to the final peak to estimate the total amount produced

**Table 1** Fitting parameters of the $CO_2$ production curves for the different incubation times and irradiation modes

| | Exponential time constant (s) | Linear slope | Intercept |
|---|---|---|---|
| 0.5 h | 242 ± 8 | | |
| 1 h | 270 ± 50 | $(2.68 ± 0.16) × 10^{-5}$ | $(1.47 ± 1.10) × 10^{-3}$ |
| 2 h | | $(1.83 ± 0.02) × 10^{-5}$ | $(1.38 ± 0.03) × 10^{-2}$ |
| 3 h | | $(1.65 ± 0.01) × 10^{-5}$ | $(7.91 ± 3.44) × 10^{-4}$ |
| 1 h-1 irr | | $(2.57 ± 0.07) × 10^{-5}$ | $(2.28 ± 0.48) × 10^{-3}$ |
| | | $(1.60 ± 0.02) × 10^{-5}$ | |

**Table 2** Estimate of the total $CO_2$ production

| Sample | 0.5 h | 1 h | 2 h | 3 h | 1 h-1 irr |
|---|---|---|---|---|---|
| Total $CO_2$ | 0.079 | 0.082 | 0.079 | 0.080 | 0.080 |

The associated error is ±4 %

## Steady or steep $CO_2$ increase

The $CO_2$ peak increases after an irradiation event either linearly or steeply. A short incubation time leads to a steep increase of $CO_2$ subsequently metabolized. Longer incubation times correspond to an initial linear increase followed by a steep increase of lesser extent up to the saturation level.

The rationalization of the "double behavior" can be made according to a few considerations.

1. The total $CO_2$ production, $CO_2$-l + $CO_2$-d (i.e., the amount obtained both by linear and by steep increase followed by a decay) is similar for all incubation times. This is an indication that the all samples absorbed the same amount of HDNS and that 0.5-h incubation time is sufficient to reach the maximum HDNS absorption by the cell. Longer incubation times affect the kinetics of the intracellular metabolism, but not the total amount absorbed.

2. In aqueous solutions, the flash photolysis of proton caged compounds is of the order of nanoseconds (Gutman et al. 1981) and the $CO_2$ generation according to equilibrium (1) has a time scale of $10^{-2}$ to $10^{-5}$ s (Schulz et al. 2006). Of the observed processes, the steep increase occurs in a time scale comparable with the flash photolysis of PCCs and $CO_2$ generation in aqueous solution, whereas the linear increase takes place on the minutes-to-hours timescale. A slow $CO_2$ increase as a result of a partial proton release is to be excluded because the behavior of the 0.5-h incubation time sample. In this case, the first irradiation event caused a steep increase of the $CO_2$ level to saturation, thus proving both that it is sufficient to convert the whole HDNS absorbed by the cells and that the photol-

ysis of the PCC is fast event on the scale of the whole $CO_2$ generation and metabolism.

3. $CO_2$-d is ready metabolized to a level similar to the one before the steep increase. At variance with this, the $CO_2$-l is not metabolized at all. The linear behavior as a result of a balance of $CO_2$ released and metabolized is to be excluded, because this would result in different total $CO_2$ production for the different incubation times.

The overall $CO_2$ production upon irradiation of HEK-293 cells dosed with HDNS for different incubation times is compatible with an HDNS confinement into intracellular vesicles of growing average size with growing incubation time, and a minimum size of 100 nm that ensures their stability (Pornpattananangkul et al. 2010). The accumulation into intracellular vesicles is a common reaction of cells to isolate intracellular exogenous agents. This is typical, for instance, for exogenous amines on mammalian cells, for which time of confinement and type of vesicle depend on several parameters, such as lipophilicity/hydrophilicity ratio, pKa, type of amine, i.e., if primary, secondary of tertiary (Dean et al. 1984). Later, it was shown that the accumulation of polyamines in Chinese hamster ovary cells proceeds in two tightly connected steps, i.e., the initial transport of the substrate across the plasma membrane into the cytosol via a classical transporter that requires rapidly followed by its sequestration in the polyamine sequestering vesicles (Soulet et al. 2004). A similar model, in our case, would explain the $CO_2$ linear increase, the lack of $CO_2$-l metabolization, and why the linear section precedes the steep increase.

The confinement of HDNS in vesicles creates a barrier between the photo-generated protons and the required $HCO_3^-$ to give rise to the $CO_2$. Therefore, although the first irradiation event is sufficient to free all protons from intracellular HDNS, the slow step of the $CO_2$ production is due to the migration either of the protons outside or the $HCO_3^-$ inside the vesicles. The latter option is more likely to occur because the subsequent $CO_2$ production would occur inside the vesicles, where it cannot be metabolized. An outward flow of protons would cause $CO_2$ production in the cellular cytosol where it could be metabolized by the CA and/or gas-channel proteins.

In this scenario, the vesicles would have a size distribution that changes with the incubation time. Factors that influence the vesicles growth after the irradiation event are the $HCO_3^-$ influx and/or $CO_2$ production, a process which may occur with the aid of the cytosolic lipid droplets to help extend the vesicle membranes. Possibly, also vesicle fusion contributes to vesicle growth, though without really playing a role in the kinetic trend. In general, vesicle fusion may occur with or without content mixing, or with a content loss, depending on the type of cargo and on the fusion mechanism (Marrink and Mark 2003). In our case, a payload loss upon fusion can be excluded, because this would imply a $CO_2$ release into the cell, with a consequent fast metabolization and deviation from the linear behavior, which is not observed. In a fusion without mixing (which would ensure the $CO_2$ confinement), the vesicles can still be treated as separate entities in kinetic terms, hence with no impact on the kinetic behavior. A fusion with mixing content would have marginal effects on the kinetic behavior because the slowing effects related to the larger size of the vesicles (i.e., longer pathway to reach the protons in the inner shells of the vesicles, after depletion of the outer shells) are compensated by the actual mixing, which partially removes the proton concentration gradients. In the latter case, only the $CO_2$-d/$CO_2$-l ratio would ultimately be influenced because a larger number of vesicles would reach the critical sizes, at a given moment, due to the fusion, and a larger amount of $CO_2$ is freed in the cell, to be metabolized with an exponential behavior ($CO_2$-d).

The vesicle growth continues until reaching a critical size range, sensitive to UV irradiation. A vesicle's variable size distribution would also explain the decreasing slope of the linear sections with the incubation time. The larger the vesicle, the longer, on average, the pathway for the $HCO_3^-$ to reach the protons, and the slower the process. The steep increase is then likely related to a disruption of the vesicles of the critical sizes, provided they are sensitive to the UV irradiation.

Free protons can then be metabolized by the cell in a similar way as for the short incubation time (0.5 h). The existence of critical size vesicles may be the cause of the small exponential for the 2-h incubation sample at the second irradiation event. In this round, only a small fraction of the vesicles reached a critical size that can be freed upon irradiation.

In order to verify the vesicle hypothesis and determine whether the irradiation event can trigger the explosion of the critical-sized ones, a test was made on a 1-h incubation sample. This sample was only initially irradiated for 1 min with UV light and then monitored by infrared spectroscopy, without any further irradiation. The integrated $CO_2$ peak area is reported in Fig. 1e and it only shows a monotonous

increase, with the same slope as for the multi-irradiated one in the same time range. Afterwards, the slope changes to a value similar to the 3-h sample until it reaches the saturation level. Therefore, we conclude that the UV irradiation is not only the trigger for the HDNS photolysis but also for the critical-size vesicle disruption.

## Conclusions

HDNS is a proton caged compound that may be used as an exogenous agent for intracellular acidification upon dosing to cells and photolysis for effect of near-UV light. This causes an increase of intracellular $CO_2$ due to the generation and decomposition of carbonic acid, which can be probed by infrared spectroscopy. The integrated $CO_2$ peak intensity displays a kinetic behavior that is a function of the incubation time, and is a combination of a linear increase and a steep increase followed by an exponential decay.

The total $CO_2$ produced is similar for all the samples, regardless of the incubation time. This implies that it is only related to the initial HDNS concentration and can be used as a probe of the overall intracellular acidification. The time scale of the process, though, changes with the incubation time and is much faster (a few minutes) for the short incubation and it is over 1 h for the longest incubation time.

The $CO_2$ peak intensity behavior is interpreted in terms of confinement of the HDNS in intracellular vesicles with an average size distribution that grows with the incubation time. The vesicles are subject to size variation upon $HCO_3^-$ influx and subsequent $CO_2$ generation according to a linear kinetic. Vesicle fusion also possibly occurs, though with an estimated marginal impact on the kinetic trend. The UV irradiation of the critical-size vesicles causes their breaking and release of the protons, which readily react and yield $CO_2$.

## References

Boron WF (2004) Regulation of intracellular pH Adv. Physiol Educ 28:160–179

Boron WF, Boulpaep EL (1983) Intracellular pH regulation in the renal proximal tubule of the salamander. Basolateral $HCO_3^-$ transport. J Gen Physiol 81:53–94

Bourque CW (2008) Central mechanisms of osmosensation and systemic osmoregulation. Nat Rev Neurosci 9:519–531

Carbone M, Zlateva T Quaroni L (2013) Monitoring and manipulation of the pH of single cells using infrared spectromicroscopy and a molecular switch. Biochim Biophys Acta Gen Subj 1830(4):2989–2993

Chegwidden WR, Dodgson SJ, Spencer IM (2000) The roles of carbonic anhydrase in metabolism cell growth and cancer in animals. Carbonic Anhydrases EXS 90(90):343–363

Chiche J, Brahimi-Horn MC, Pouysségur J (2010) Tumour hypoxia induces a metabolic shift causing acidosis: a common feature in cancer. J Cell Mol Med 14:771–794

Choi I, Aalkjaer C, Boulpaep EL, Boron WF (2000) An electroneutral sodium/bicarbonate cotransporter NBCn1 and associated sodium channel. Nature 405:571–575

Dean RT, Jessup W, Roberts CR (1984) Effects of exogenous amines on mammalian cells, with particular reference to membrane flow. Biochem J 217:27–40

Deitmer JW, Schlue WR (1989) An inwardly directed electrogenic sodium-bicarbonate co-transport in leech glial cells. J Physiol 411:179–194

Dodgson SJ, Forster RE II, Storey BT, Mela L (1980) Mitochondrial carbonic anhydrase. Proc Natl Acad Sci USA 77(9):5562–5566

Endeward V, Cartron JP, Ripoche P, Gros G (2008) RhAG protein of the Rhesus complex is a $CO_2$ channel in the human red cell membrane. FASEB J. 22:64–73

Finbow ME, Harrison MA (1997) The vacuolar $H^+$-ATPase: a universal proton pump of eukaryotes. Biochem J 324:697–712

Gutman M, Dan Huppert P, Pined E (1981) The pH jump: a rapid modulation of pH of aqueous solutions by a laser pulse. J Am Chem Soc 103:3709–3713

Harvey BJ, Eherenfeld J (1988) Role of Na exchange in the control of intracellular pH and cell membrane conductances in frog skin epithelium. J Gen Physiol 92:793–810

Hulikova A, Vaughan-Jones RD, Swietach P (2011) Dual role of $CO_2$/$HCO_3^-$ buffer in the regulation of intracellular pH of three-dimensional tumor growths. J Biol Chem 286(16):13815–13826

Itel F, Al-Samir S, Öberg F, Chami M, Kumar M, Supuran CT, Deen PMT, Meier W, Hedfalk K, Gros G, Endeward V (2012) $CO_2$ permeability of cell membranes is regulated by membrane cholesterol and protein gas channels. FASEB J. 26:5182–5191

Kabalka GW, Varma M, Varma RS, Srivastava PC, Knapp FF Jr (1986) Tosylation of alcohols. J Org Chem 51(12):2386–2388

Kustu S, Inwood W (2006) Biological gas channels for $NH_3$ and $CO_2$: evidence that Rh (Rhesus) proteins are $CO_2$ channels. Transfus Clin Biol 13:103–110

Lagadic-Gossmann D, Huc L, Lecureur V (2004) Alterations of intracellular pH homeostasis in apoptosis: origins and roles. Cell Death Differ 11:953–961

Marrink SJ, Mark AE (2003) The mechanism of vesicle fusion as revealed by molecular dynamics simulations. J Am Chem Soc 125:11144–11145

Obara M, Szeliga M, Albrecht J (2008) Regulation of pH in the mammalian central nervous system under normal and pathological conditions: facts and hypotheses. Neurochem Int 52(6):905–919

Orlowski J, Kandasamy RA, Shull GE (1992) Molecular cloning of putative members of the Na/H exchanger gene family. J Biol Chem 267(13):9331–9339

Overton E (1895) Über die osmotischen Eigenschaftender lebenden Pflanzen und Tierzelle. Vierteljahrsschr Naturforsch Ges Zürich 40:159–201

Pedersen PL, Carafoli E (1987) Ion motive ATPases. Ubiquity, properties, and significance to cell function. Trends Biochem Sci 12:146–150

Pornpattananangkul D, Olson S, Aryal S, Sartor M, Huang C-M, Vecchio K, Zhang L (2010) Stimuli-responsive liposome fusion mediated by gold nanoparticles. ACS Nano 4:1935–1942

Pouysségur J, Sardet C, Franchi A, L'Allemain G, Paris S (1984) A specific mutation abolishing $Na^+$/$H^+$ antiport activity in hamster fibroblasts precludes growth at neutral and acidic pH. Proc Natl Acad Sci 81:4833–4837

Romero MF, Hediger MA, Boulpaep EL, Boron WF (1997) Expression cloning and characterization of a renal electrogenic $Na^+$/$HCO_3^-$ cotransporter. Nature 387:409–413

Romero MF, Henry D, Nelson S, Harte PJ, Dillon AK, Sciortino CM (2000) Cloning and characterization of a $Na^+$ driven anion exchanger (NDAE1): a new bicarbonate transporter. J Biol Chem 275:24552–24559

Schulz KG, Riebesell U, Rost B, Thoms S, Zeebe RE (2006) Determination of the rate constants for the carbon dioxide to bicarbonate inter-conversion in pH-buffered seawater systems. Mar Chem 100:53–65

Soulet D, Gagnon B, Rivest S, Audette M, Paulin R (2004) A fluorescent probe of polyamine transport accumulates into intracellular acidic vesicles via a two-step mechanism. J Biol Chem 279:49355–49366

Thwaites DT, Anderson CMH (2007) $H^+$-coupled nutrient, micronutrient and drug transporters in the mammalian small intestine. Exp Physiol 92(4):603–619

Wang CZ, Yano H, Nagashima K, Seino S (2000) The $Na^+$-driven $Cl^-$/$HCO_3^-$ exchanger. J Biol Chem 275:35486–35490

Wong P, Kleemann HW, Tannock IF (2002) Cytostatic potential of novel agents that inhibit the regulation of intracellular pH. Br J Cancer 87:238–245